Novel Energy Management System for a DC MicroGrid

Ashan Imantha Bandara[1], Prabath Binduhewa[2], Lilantha Samaranayake[3], Janaka Ekanayake[4]

Dept. of Electrical Eng.

University of Peradeniya

Peradeniya, Sri Lanka

e-mail: 1. ashanimhb31@gmail.com; 2. prabath@ee.pdn.ac.lk; 3. lilantha@ee.pdn.ac.lk; 4. jbe@ee.pdn.ac.lk

Abstract—This paper presents a design and simulation of a rule based energy management system for a dc MicroGrid that considers a cost function to reflect the battery degradation and that relates to the actual battery parameters. The derivation of the battery cost function and the utilization of that to ensure an optimum utilization of the battery energy storage were presented. The detailed description of the algorithms used to implement the EMS was presented. Simulation on PSCAD/EMTDC software was used to demonstrate the operation of the EMS both under grid connected and islanded modes. Further, the inertia support provided by the super-capacitor to avoid the collapse of the dc link of the MicroGrid was demonstrated.

Keywords - MicroGrid; EMS; battery; super-capacitor

_____*****_____

I. INTRODUCTION

The adverse effects to the environment caused by burning of fossil fuel and depletion of fossil fuel triggered to search for alternative electricity generation sources. As an alternative, renewable energy sources such as photovoltaics and wind are now emerged as main stream power generation sources. As the renewable energy resource is intermittent and variable, they have introduced challenges in terms of maintaining voltages, line flows and stability of utility networks. In order to overcome some of these challenges MicroGrids have been considered. A MicroGrid is a low-voltage power system, smaller in capacity, consisting local generation and local loads with ability to operate autonomously or grid connected modes [1]-[4]. Customer point of view, MicroGrid improves the reliability of power whereas from the utility point of view, MicroGrid enables to connect higher percentage of renewables without destabilizing the existing utility network. In order to facilitate the stable operation of a MicroGrid under autonomous mode, energy storage within the MicroGrid is essential.

Even though early MicroGrids consist of ac feeders, only dc MicroGrids and hybrid MicroGrids are emerging [1]-[4]. There are two main reasons to attract interest for dc MicroGrids [1], [5]-[7]. Renewable energy sources such as PV and energy storage produce dc voltages. In order to integrate them to ac MicroGrid, a dc-dc-ac conversion stage is essential. Further, many loads such as ICT equipment, entertaining equipment, portable appliances, etc. operates on dc internally thus requiring ac-dc(-dc) conversion stages when connecting to the ac MicroGrid.

A dc MicroGrid consists of number of microsources (<500 kW) such as PV systems, wind turbines, and fuel cells [8], [9]. These microsources integrated to the MicroGrid through single-stage power conversion stage (often dc-dc). The utility interconnection should allow bi-directional power flow thus requiring a bi-directional ac-dc converter. The dc MicroGrid also requires energy storage to overcome the transient in the system and to negate medium or long term demand-supply mismatches. Supercapacitors and flywheels are used to overcome the transients within the MicroGrid while battery storage is used for medium or long term demand supply matching [10]-[14].

Hierarchical control that incorporates tertiary, secondary and primary control stages are usually employed for a dc MicroGrid. Primary control, which refers to the droop-control, responds to the parameters set by the secondary control such that the voltage is maintained within the acceptable values. Secondary control ensures that the power shared by each source is in accordance with the values scheduled by the tertiary control. Tertiary control refers to the Energy Management System (EMS) that uses a rule-based system or an optimization routine based on cost or loss optimization to schedule different constituent parts of the MicroGrid.

Different EMSs are discussed in the literature. In [15] an EMS for an ac MicroGrid is presented. Six operating modes were defined based on the grid voltage and frequency. A rule based EMS was used to select the most appropriate operating mode that schedules the utility power exchange, energy storage, and renewable energy sources. In [16] an EMS application for a dc MicroGrid established in an office building is presented. The power balance is used as the decision making variable and the carbon emission is optimized. In [17] an EMS based on a rule based decision making system is implemented for an isolated dc MicroGrid. An EMS with layered architecture is presented in [18]. The topmost layer is the human machine interface. The next layer, the prediction layer, used metadata to predict the load and source profiles. Then the energy management layer defines the schedules and the

operating layer sends the commands according to the schedule given by the energy management layer. The operating layer is developed as a rule based system. Considering two types of dc MicroGrid configurations, distributed energy resources with lumped loads and distributed energy resources with distributed loads, reference [19] presents a rule based EMS. An EMS with fuzzy control for a dc MicroGrid is presented in [20]. Here in order to improve the life cycle of the battery, the fuzzy controller manages the desired state of charge of the battery. A complex EMS considering a multi-objective optimization with forecasting of resources is presented in [21]. Except in [21], none of the other EMS implementations considered the detail

model for the degradation of the energy storage device due to constant charging and discharging. Even though [21] considered a cost function to reflect battery degradation, it is depending on a number of unknown constants which are not related to the actual battery parameters. Considering the simplicity of the rule based system, in this paper an EMS was developed using a rule based system while considering a cost function that reflects the battery degradation and that related to the actual battery parameters. Further a super-capacitor was used for inertia support.
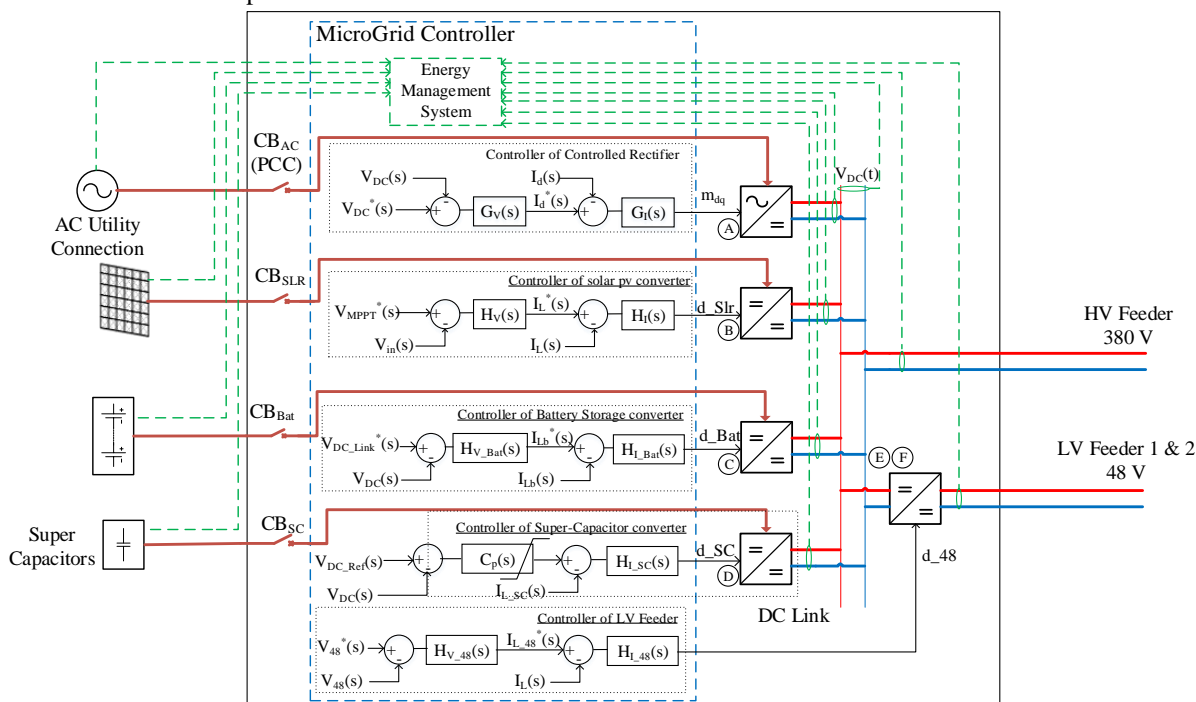

Figure 1. Proposed dc MicroGrid topology

II. MicroGrid Platform

The proposed MicroGrid is shown in Fig. 1. It has solar photovoltaic (PV) as local generation, connected to the utility ac grid, a battery and a super-capacitor as energy storage system (ESS) elements and two feeders to local loads.

The utility interface determines the power exchange between the MicroGrid and the ac utility network. Thus when there is a deficit power in the MicroGrid the controller will use converter A to import power from the ac utility network. Conversely when there is excess power, controller of converter A will export power from MicroGrid to ac utility. This is done by a reference, Rf_{Grid}, received from the EMS to the power regulation controller (this is not shown in Fig. 1).

As Solar PV is a non-conventional renewable energy source, the controller of the PV system extracts the maximum available power at a given instance and rarely reduces the output from the available maximum. Occasionally

PV output is shed through a reference, Rf_{PV}, received from the EMS.

The battery storage is assigned to supply steady state power requirement as scheduled by the EMS in both grid connected and islanded modes. Converter C charges the battery when there is excess power and discharges when there is a power shortage in the dc MicroGrid. This is done by a reference, Rf_{Bat}, received from the EMS.

Thus super-capacitor is assigned to supply the rapid power demands of the MicroGrid. Due to the variations in loads and sources dc link voltage varies. This voltage variation includes both transient and steady state components. However, when the EMS maintaining the power balance the variation of the dc link is mainly transient variations and the super-capacitor is controlled by an outer loop that maintains the dc link voltage to a reference. As energy can be extracted from the super-capacitor relatively

fast, the above control action also provides inertia support to the dc MicroGrid.

III. COST FUNCTION OF THE BATTERY

A. Battery model

The battery model described in reference [22] was adopted for this study. The model is shown in Fig. 2. It is based on an feedback loop that computes the internal battery voltage based on (1):

$$E_{bat} = E_0 - K\frac{Q}{Q - \int_0^t I_{bat}\,dt} + Ae^{\left(-B\int_0^t I_{bat}\,dt\right)} \tag{1}$$

where in (1) and Fig. 2,

E_{bat} = No load voltage (V)

E_0 = Battery Constant Voltage

K = Polarization Voltage (V)

Q = Battery Capacity (Ah)

$\int_0^t I_{bat}\,dt$ = Utilized Battery charge (Ah)

A = Exponential zone amplitude (V)

B = Exponential zone charge constant (Ah-1)
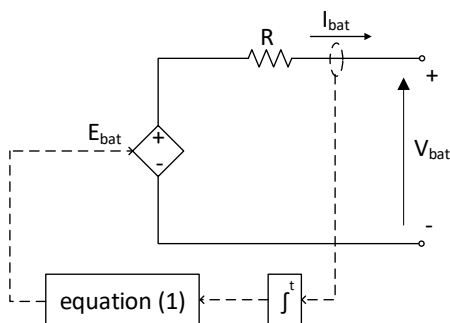
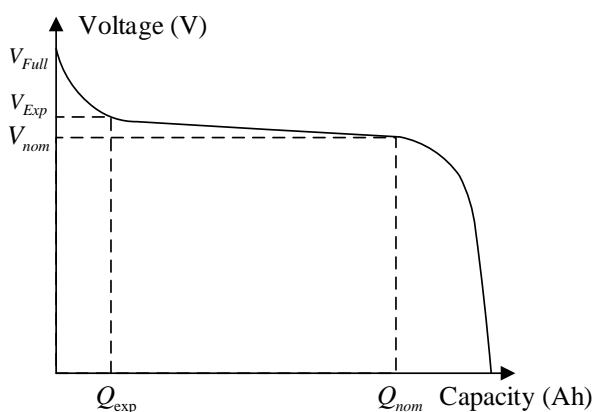V_{bat} = Battery terminal voltage

Figure 2. Battery model

Figure 3. Typical discharge curve

R = Internal Resistance

I_{bat} = Batter current

The battery constant voltage, E_0, is given by:

$$E_0 = V_{Full} + K + RI_{bat} - A \tag{2}$$

The polarization voltage, K, is given by:

$$K = \frac{V_{Full} - V_{nom} + A\left(e^{-B.Q_{nom}} - 1\right)\left(Q - Q_{nom}\right)}{Q_{nom}} \tag{3}$$

The different values of (3) can be obtained from the typical discharge curve shown in Fig. 3.

The Exponential zone amplitude, A, and exponential zone charge constant, B are given by:

$$A = V_{Full} - V_{Exp} \tag{4}$$

$$B = \frac{3}{Q_{Exp}} \tag{5}$$

The internal Resistance of the battery is given by [23]:

$$R = \frac{V_{nom}\left(1 - \eta\right)}{C_{rate}.Q_{Exp}} \tag{6}$$

where

η = Efficiency of the battery

C_{rate} = discharge current multiplier

B. Cost function

Every time the battery charges and discharges, it is being degraded. The state-of-charge (SOC), state-of-health (SOH) and depth-of-discharge (DOD) of the battery are the main factors that determine the degradation of a battery. These parameters reflect the effects of operating temperature, operating current and terminal voltage of the battery. In order to decide whether to take the power from the grid or from the battery, a cost function that reflects the degradation of the battery was derived. This was based on reference [24].

The cost of energy usage of a battery is given by:

$$F_d = C_{bat}\left[P_d - P_{Ld}\right]\text{ in S/hr} \tag{7}$$

where

C_{bat} is the cost of utilizing the battery in \$/kWh

P_d is the discharging power

P_{Ld} is the losses incorporated with discharging operation

The cost of utilizing the battery is given by:

$$C_{bat} = C_{Charg} + C_{Avail} \tag{8}$$

where

C_{Charg} is the cost of charging the battery

C_{Avail} is the availability cost which is the cost of keeping 1 kWh storage capacity available.

If renewable energy is purely used for charging the battery C_{Charg} can be considered as zero. Thus C_{Avail} is the cost incorporated with the battery usage and is given by:

$$C_{Avail} = \frac{Replacement\ Cost}{C_\Sigma} \tag{9}$$

where

C_Σ is the total life time cycling capacity of the battery

The total life time cycling capacity, C_Σ, of the battery depends on the rated capacity of the battery (C_r), rated depth-of-discharge (DOD_r) and life time in terms of cycles (L_r). For a Li-Ion battery C_Σ is given by (10).

$$C_\Sigma = C_r \times DOD_r \times (0.9L_r - 0.1)` \tag{10}$$

The number of cycles for Li-Ion batteries is given as a curve in [25]. From curve fitting (11) was obtained to represent L_r.

$$L_r = \exp\left(\frac{4.98 - \ln(DOD_r)}{0.685}\right) \tag{11}$$

The losses associated with the discharging the battery (shown in (7)) is given by

$$P_{Ld} = \alpha(P_d)^2 + \beta(P_d) \tag{12}$$

where

$$\alpha = \left\{R + \frac{K}{SOC(t)}\right\}\frac{1}{V_r^2}$$

$$\beta = \frac{C_r . K\{1 - SOC(t)\}}{V_r^2 SOC(t)}$$

K and R are as defined in equations (3) and (6)
V_r is the rated voltage of the battery

IV. PROPOSED EMS SYSTEM

The proposed EMS system is implemented as a real time operating algorithm. Before commencing the algorithm a set of variables are initiated inside the EMS.

Prior to selecting the most suitable operating mode, the EMS algorithm first check the status of the utility grid ($Grid_{Sts}$) to determine whether the MicroGrid is in grid connected mode ($Grid_{Sts}$ =1) or in islanded mode ($Grid_{Sts}$ =0). Next it checks the power balance (P_{Bal}) between solar PV (P_{PV}) and Load (P_{Ld}) using equation (13):

$$P_{Bal} = P_{PV} - P_{Ld} \tag{13}$$

Depending on the power balance and availability of the utility the EMS decides four operating modes as shown in

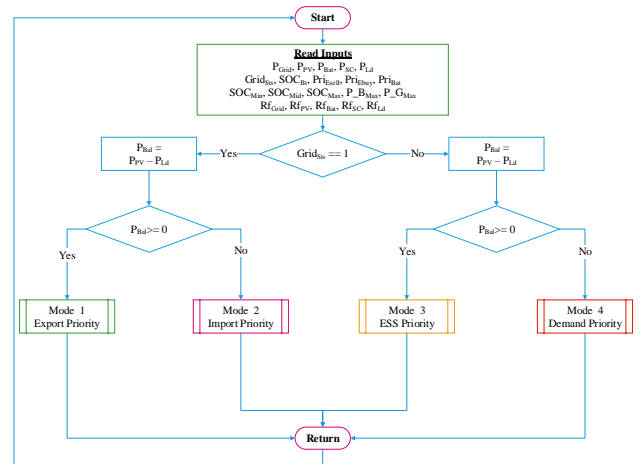Fig. 4. Inputs shown in Fig. 4 are described under each operating mode.

Figure 4.   The block diagram of the Proposed EMS

A. Export Priority Mode

The algorithm used for this mode is shown in Fig. 5. The EMS will first evaluate the state-of-charge of the battery (SOC_{Bat}). If SOC_{Bat} is less than the maximum allowable SOC level, SOC_{Max}, then the excess power is used to charge the battery. The condition $SOC_{Bat} < SOC_{Max}$ is referred to as SOC constraint in subsequent sections. While maintaining the rated depth-of-discharge the SOC_{Max} limit can be adjusted to shift the charging profile of the battery. Before scheduling the charging power of the battery, EMS checks the power rating of the converter C (Fig. 1). If the excess power is more than the rated power (P_B_{Max}) of the battery interface converter, the EMS will schedule the battery charging power reference (Rf_{Bat}) to maximum. Otherwise it will schedule the battery to charge using the available power. Once the battery is fully charged then the battery interface converter goes into idle state. Then the EMS checks the possibility of exporting available power to the ac utility. If the excess power is more than the rating of the ac utility interface converter (A), P_G_{Max}, the EMS schedules the export power (Rf_{Grid}) to be the maximum and initiate a PV shedding scheme in order to keep the power balance within the MicroGrid. The amount of PV to be shed was calculated using (14).

$$Rf_{PV} = (|P_{Grid}| + |P_{Ld}|) \tag{14}$$

B. Import Priority Mode

In the grid connected mode if the total local load is more than PV generation, the EMS shifts to the import priority mode. The controlled rectifier is scheduled to import power from the ac utility or battery interface converter is scheduled to discharge and supply the power to keep the power balance

145

_____

inside the dc MicroGrid. Further in this mode battery is charged if the utility Time of Use (ToU) price is minimum.

In this mode the scheduling is primarily done according to the cost of importing power from the ac utility ($C_{Utility}$), and the cost involved in discharging the battery (C_{bat_d}). The ac utility price, $C_{Utility}$, is the selling price of the energy from service providers to the MicroGrid and assumed as a ToU tariff. The cost of discharging the battery was computed using (7) by multiplying F_d with the time step of each iteration.
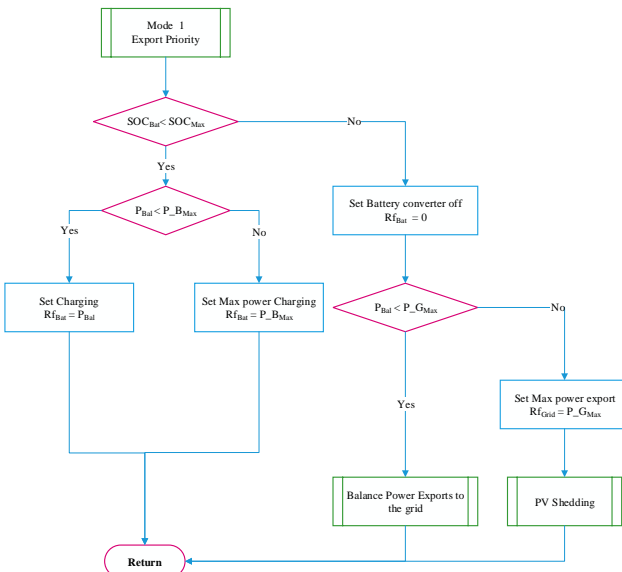
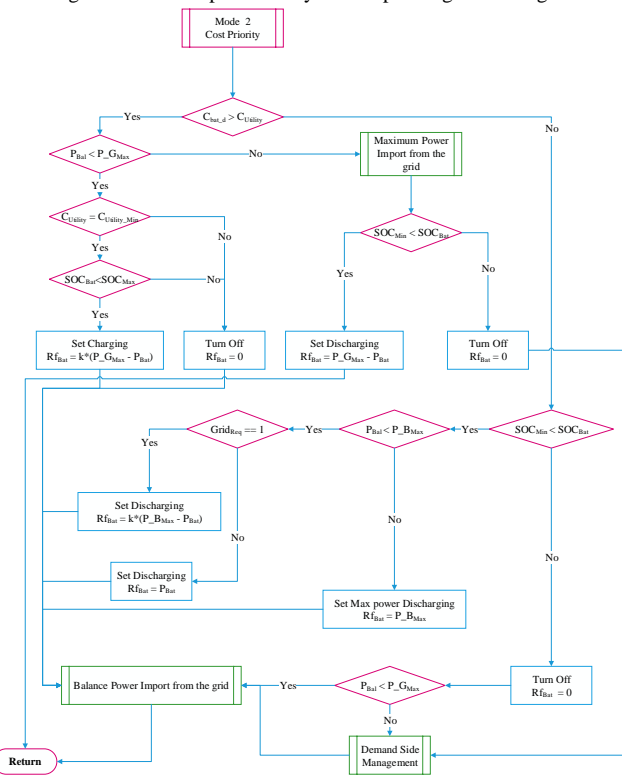Figure 5.   The Export Priority mode operating block diagram

Figure 6.   Block diagram of Import Priority Mode

The algorithm used for this mode is shown in Fig. 6. Initially algorithm checks whether $C_{Bat\_d} > C_{Utility}$; in other wards whether the cost of importing power from the grid is less than the discharging the battery. If the battery energy cost (C_{bat_d}) is more than ($C_{Utility}$), the EMS will import power from the ac utility. To proceed further the EMS checks whether the power balance is less than the rating of the controlled rectifier (P_G_{Max}). Then EMS checks whether the utility energy price is the minimum price of ToU ($C_{Utility\_Min}$). Also it checks the SOC constraint. The desired charging power of the battery is set according to (15) where k is a constant used to ensure that the total import power is within P_G_{Max}.

$$Rf_{Bat} = k_c \left(P\_G_{Max} - P_{Bal} \right) \;; 0 \le k_c \le 1 \qquad (15)$$

Further, the balance power is imported from the ac utility through the utility interface converter. On the other hand if the P_{Bal} is more than P_G_{Max}, the algorithm examines whether the battery has sufficient charge, i.e. $SOC_{Min} < SOC_{Bat}$, to supply the demand that cannot be supplied solely by importing power from the ac utility. Then the battery converter is scheduled to discharge mode according to (16). However if batter doesn't have enough charge then the demand side management (DSM) is initiated to maintain power balance.

$$Rf_{Bat} = P\_G_{Max} - P_{Bal} \qquad (16)$$

Conversely when the extracting energy from the battery C_{bat_d} is cheaper than utility price, $C_{Utility}$, the EMS will schedule the battery storage to supply the demand instead of utility interface. However the dc link control is handled by the utility interface converter.

Firstly the controller checks whether $SOC_{Min} < SOC_{Bat}$. If the battery has sufficient SOC, then the converter rating is checked against P_{Bal}. If the rating is adequate then P_{Bal} is supplied by discharging the battery. However in an instance where the ac utility operator requests support from the MicroGrid, it is going to act as a good citizen. So in Import priority mode when the battery energy is cheaper it checks whether ac utility request support ($Grid_{Req} = 1$). In such situation the battery is scheduled according to (17)in order to increase the rate of discharge and sell electricity to the ac utility.

$$Rf_{Bat} = k_d \left(P\_B_{Max} - P_{Bal} \right) \;; 0 \le k_d \le 1 \qquad (17)$$

Further, in import priority mode the utility interface converter is primarily importing power from the utility or keep in idle while controlling the dc link. However if ac

146

_____

utility require support then it exports the required amount of power from dc MicroGrid to ac utility.

C. Energy Storage System (ESS) Priority Mode

ESS Priority mode occurs during islanding ($Grid_{Sts}=0$) where the MicroGrid has excess power (P_{Bal} is positive). Since there is no grid connection there is no opportunity to keep the power balance within the MicroGrid by exporting available excess power. Only possibility is to use the excess power to charge the battery. It also checks whether the battery is overcharged. Fig.7 shows the block diagram of the ESS priority mode.

When ESS priority mode is initiated, first it inspects the SOC constraint of the battery. If this condition satisfied, the EMS check the excess power against the power rating of the battery converter. When the available power is less than power rating of the Converter C, the battery is set to charge using P_{Bal}.
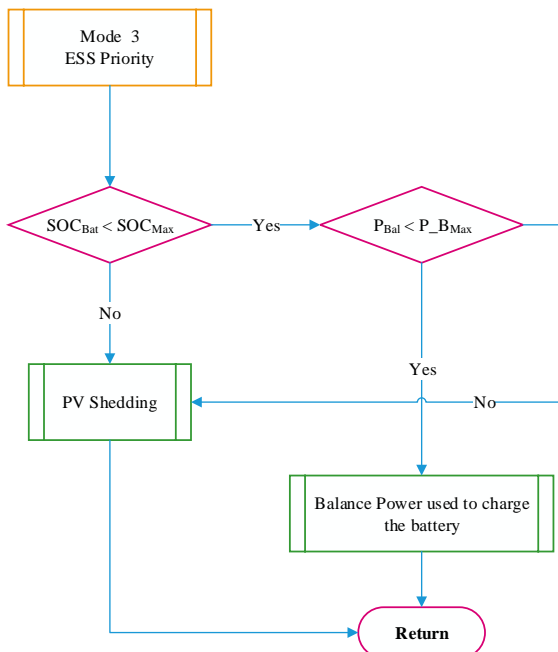

Figure 7.   Block diagram of ESS Priority Mode

Otherwise it charges at the maximum rating of the converter. However one or both constraints in relation to SOC or converter rating fail then to ensure the power balance PV shedding is initiated to spill the unused excess power. The amount of PV to be shed was calculated according to (18).

$$Rf_{PV} = \left(\left| P_{Bat} \right| + \left| P_{Ld} \right| \right) \qquad (18)$$

In the islanded mode, the battery storage controls the dc link voltage. Similar to the operation of the utility interface converter in grid connected mode, the battery interface converter cannot be scheduled directly to reference power levels. Instead the other converter (solar PV and load

interface) are scheduled to operate while maintaining the power balance in islanded dc MicroGrid. Thus the reference power of the battery interface converter (Rf_{Bat}) is automatically adjusted to P_{Bal}.

D. Demand Priority Mode

The fourth operating mode of the EMS is the demand priority mode. This is the most critical operating condition of the dc MicroGrid. The demand priority mode is activated in islanded mode when the P_{Bal} is negative. Thus in this mode the high priority is given to ensure the uninterrupted supply to the loads and stability of the MicroGrid. The corresponding block diagram is given in Fig. 8.
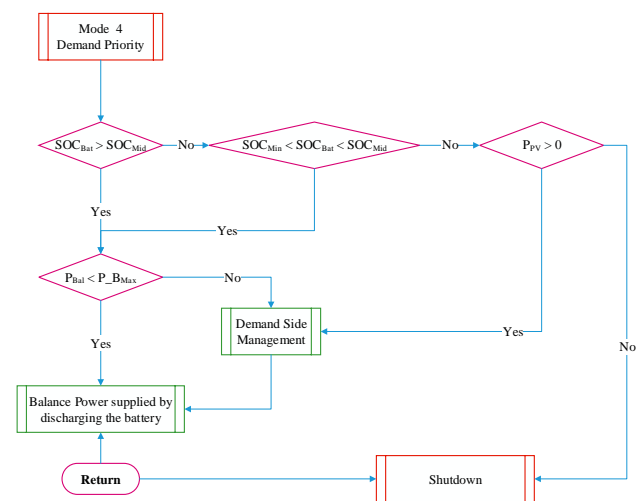

Figure 8.   Block diagram for Demand Priority Mode

First the SOC of the battery, SOC_{Bat}, is checked against a predefined SOC level, SOC_{Mid}. If the constraint, $SOC_{Mid} < SOC_{Bat}$ is satisfied then the power rating of the Converter C is checked by the EMS. If require power demand is more than the battery interface converter rating then the demand side management is started. Otherwise MicroGrid operates normally while supplying the demand by discharging the energy storage together with available PV.

When constraint given by $SOC_{Mid} < SOC_{Bat}$ fails then the following constraint is checked by the EMS to avoid deep discharging of the battery:

$$SOC_{Min} < SOC_{Bat} < SOC_{Mid} \qquad (19)$$

If the SOC of the battery is within the limits, the EMS initiates DSM protocol and sheds unwanted loads to increase the operating duration of the dc MicroGrid. Moreover if this constraint fail, in other words that there is not enough charge to deliver require power using the battery, the EMS inquires whether PV is available to supply at least a certain amount of

147

loads. Depending upon the amount of PV availability the DSM algorithm adjusts the loads of the MicroGrid.

Eventually if there is neither PV nor SOC available EMS send a shutdown signal and MicroGrid controller initiates the shutdown sequence to halt the operations of the dc MicroGrid.

E. Demand Side Management (DSM)

As explain before in import priority mode and demand priority mode the Demand Side management is used to schedule available power in the dc MicroGrid. Five DSM protocols were defined and they were activated according to the EMS decisions. The amount need to reduce from loads are calculated in grid priority mode using (21) and in islanded mode using (22). The new power reference value for load feeders is set according to (23).

$$Ld_{Shd} = P_{Ld} - (|P_{Grid}| + |P_{Bat}| + |P_{PV}|) \qquad (21)$$

$$Ld_{Shd} = P_{Ld} - (|P_{Bat}| + |P_{PV}|) \qquad (22)$$

$$Rf_{Ld} = P_{Ld} - Ld_{Shd} \qquad (23)$$

The DSM modes are given in Table 1.

TABLE I.   DSM GUIDELINES

DSM Mode	Description
1	The load feeder converter will be scheduled using (21) and (23).
2	The load feeder converter will be scheduled using (22) and (23).
3	The total load will be reduced to 75% of the predicted.
4	The total load will be reduced to 50% of the predicted.
5	The total load will be reduced to 25% of the predicted.

V. CASE STUDY

Two case studies have been conducted to investigate the performance of the dc MicroGrid with the same PV and load profiles. First case study was done for a grid connected MicroGrid and the second case study was done with grid failure scenario. Using the case studies performance of the dc MicroGrid with EMS was evaluated.

A. Load Profile

The proposed dc MicroGrid was assumed as a commercial building. Thus the load profile shown in Fig. 9 was used (extracted from a real building). It is worth noting that the night time load was very small compared to the day time load.

B. PV Profile

The Power generated from solar PV in a typical day is shown in Fig. 10. This curve was generated using field measurements at the same building from which the load profile was obtained.

C. Utility Energy Price

ToU price was assumed as the utility selling price. From 06.00 to 10.30 and from 12.30 to 19.00, energy price is SLR 25/kWh; from 10.30 to 12.30 it is SLR 30/kWh; from 19.00 to 22.00 it is SLR 54/kWh; and for the remaining period it is SLR 13/kWh.

D. Case Study 1

The first case study was done for a normal day operation. In order to match the simulations with real world system it was considered that 15 min in real system is equal to 0.25 sec in simulation. Thus a full day is represented by 24.5 sec. An initial delay of 0.5 sec was introduced to complete the start-up process. The details of the battery is given in Appendix A.

Since this case study is primarily a grid connected operation, the EMS works on the export priority and import priority modes. The scheduling is done by considering the utility tariff, battery discharge cost and the SOC of the battery. As explained before, the super-capacitor wascontrolled to maintain the battery voltage transiently.
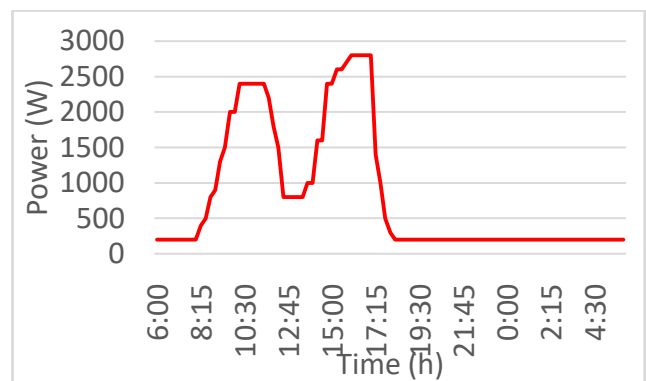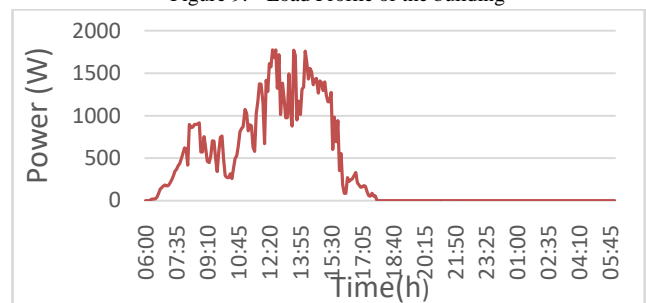
Figure 9.   Load Profile of the building

Figure 10. Variation of solar PV

Simulations were carried out to observe the performance of the MicroGrid controllers and converters. The results are presented in Fig. 11.

Fig. 11 (a) and (b) shows the variation of load and PV generation. Both followed, the profiles presented in Fig. 9 and 10.

The variation of power supplied from controlled rectifier and battery interface converter are presented in Fig.11 (c) and (d) respectively. As shown in Fig. 11 (c) during 0.5 sec to 5 sec period, most of the power was imported from the ac utility to the dc MicroGrid through the controlled rectifier. This period is equal to 6:00 h to 10:30 h in real time. The solar PV generation was less than the total load in this duration. After that from 5 sec to 6.75 sec (i.e. from 10:30 h to 12:15 h) the utility tariff increased more than the battery energy cost. Therefore the battery converter was activated and supplied majority of required power demand. The power imported from the ac utility is reduced by the utility interface converter in order to maintain the power balance. However after 6.75 sec (i.e. after 12:15 h) again utility energy price decreases compare to battery energy price. Also the solar irradiance increased more than the total load. Hence the EMS schedules the battery to charge mode. So the MicroGrid controller switched the battery interface converter to the charge mode and the SOC of the battery reaches to its maximum limit (not shown in Fig 11) at 9.00 sec (i.e. at 14.30h). After that the battery converter is put into idle and the utility interface converter and the PV converter supplied the demand. At 13.50 sec (i.e. at 19.00 h) another tariff increment appears in the ac utility energy price. Hence the MicroGrid controller sets the controlled rectifier to export power since the EMS schedules the battery interface converter to discharge the battery and support the utility grid during its peak demand. After battery reached to its critical SOC level this operation stopped (15.25 sec, i.e.at 21.00 h) and the controlled rectifier import power from the ac utility to supply the base load. At 17 sec (i.e. at 22:15 h) the imported power increased because EMS scheduled the battery converter to charge the battery to ready for the next day.

Fig. 11 (d)shows the power variation of the battery interface converter. With reference to the aforementioned discussion, in 5 sec to 6.75 sec (i.e. from 10:30 h – 12.15 h) period the battery converter started to supply power by discharging the battery. From 6.75 sec to 9 sec because of the reduction of load, the battery converter sets back to charging mode and charge the battery using the excess solar power without exporting to the ac utility. In between 9 – 13.50 sec
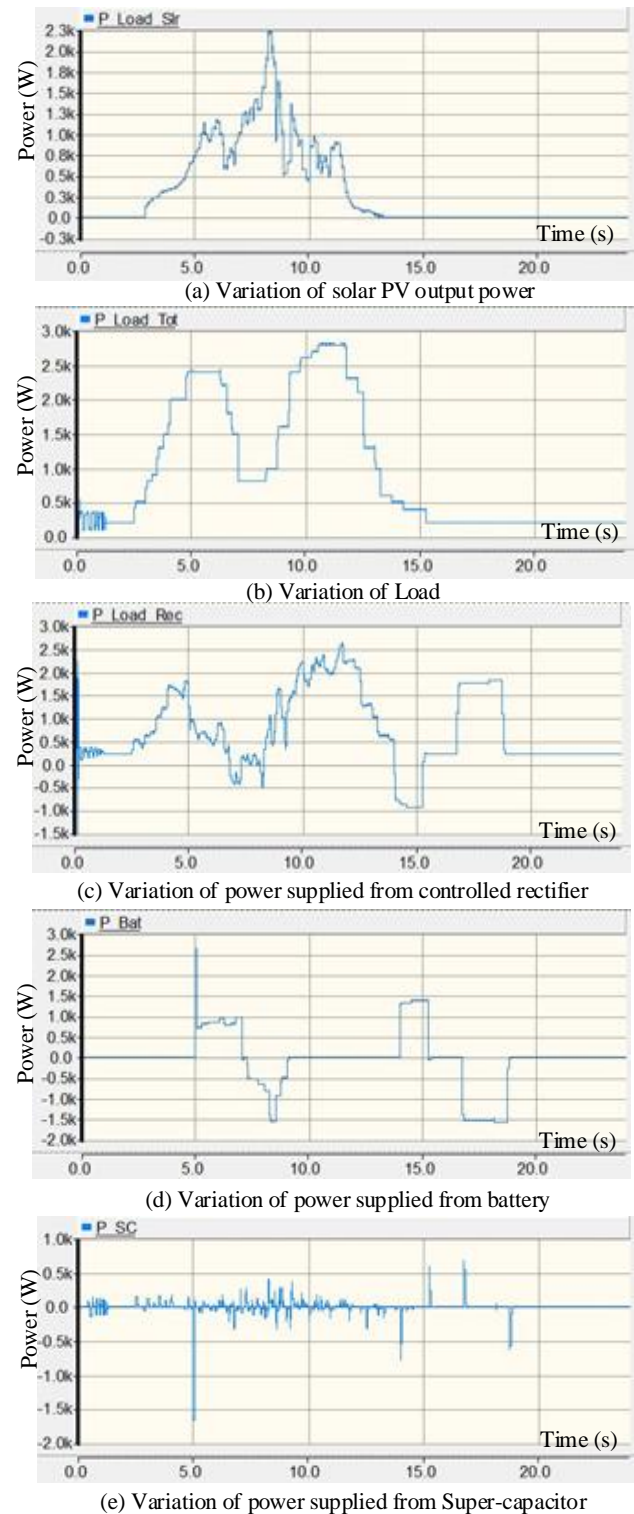

(a) Variation of solar PV output power

(b) Variation of Load

(c) Variation of power supplied from controlled rectifier

(d) Variation of power supplied from battery

(e) Variation of power supplied from Super-capacitor

Figure 11. Variations of the utility tariff and output power in case study 1

(i.e. from 14.30 h to 19.00 h), the batteryconverter set into idle mode by the controller since most of the demand was supplied from the controlled rectifier. From 13.50 sec (i.e. at 19:00 h) onwards the battery converter scheduled to be in the grid support mode.

The role of the super-capacitor is to supply the power deficit and absorbs excess by looking at the variation of the

149

dc link voltage. At every instance it charges and discharges by supplying required power difference. This variation is presented in Fig. 11 (e). Because of this the stresses of the controlled rectifier which controls the dc link voltage is reduced and the dc link voltage becomes more stable.

E. Case Study 2

In the second case study, a scenario when grid failure occurred was analyzed. The grid failure condition was simulated by disconnecting the MicroGrid from the ac utility and the controlled rectifier was put into a current controlled mode with zero current reference. Two grid failures, one at 08.36 h and restored at 09.12 h, and the other at 11.12 h and restored at 13.18 h, were considered.

The same PV profile as shown in Fig 10 was considered in this case study as well. Even though the same loading pattern shown in Fig. 9 was used, during the period of the grid failure, the load was reduced through DSM. Fig. 12 shows the resulted power profiles of the dc MicroGrid.

By comparing Fig. 9 and 10, it can be noticed that, at the first grid failure (at 3.1 sec (08.36 h)) the PV generation is more than the load. Thus EMS switched to the ESS priority mode and used the excess energy to charge the battery. Once grid is available after 0.6 s (18 min) the EMS switched back to the grid connected mode. In the second grid failure at 5.7 sec (i.e. at 11.12h) since the total load is more than the available PV generation, EMS switched back to islanded mode with the demand priority mode. Hence when SOC reaches its mid-level, the DSM scheme is activated and reduced the load. This load reduction can be observed by comparing Fig. 9 and Fig 12 (a).

Fig 12 (b)shows the variation of power supplied by the controlled rectifier. According to the figure from 3.1 sec to 3.7 sec (i.e. from 08:36 h to 09:12 h) and from 5.7 sec to 7.8 sec (i.e. from 11:12 h to 13:18 h), the controlled rectifier doesnot exchange power due to the grid failure. At this instant where the MicroGrid lost utility power, the super-capacitor converter is activated and it supplied power to the MicroGriduntil the battery converter was activated and started to supply power to stabilize the dc MicroGrid.

Furthermore, by looking at Fig 12 (c) at 3.1 sec (i.e. at 08:36 h) and at 5.7 sec (i.e. at 11:12 h), it can be seen that the battery converter took the control of dc link stability and started to supply power. During these intervals the EMS operated in the ESS priority mode and demand priority mode.In demand priority mode, the EMS used SOC as one of the decision making variable. Once the SOC of the battery storage started to reduce below SOC_{Mid} the EMS initiates the DSM algorithms. At 6.10 sec (i.e. at 11:36 h) SOC reached to $SOC_{Mid}$and DSM schedule is activated by the EMS thus reducing the load. When the grid came back at 7.8 sec (i.e. at 13:18 h), loads are restored and the dc link control was handed over to the controlled rectifier.

During the islanding process, the dc link voltage control of the MicroGrid is transferred to the battery converter from the controlled rectifier. However the EMS signals were

(a) Variation of Load power

(b) Variation of power supplied from controlled rectifier

(c) Variation of power supplied from battery
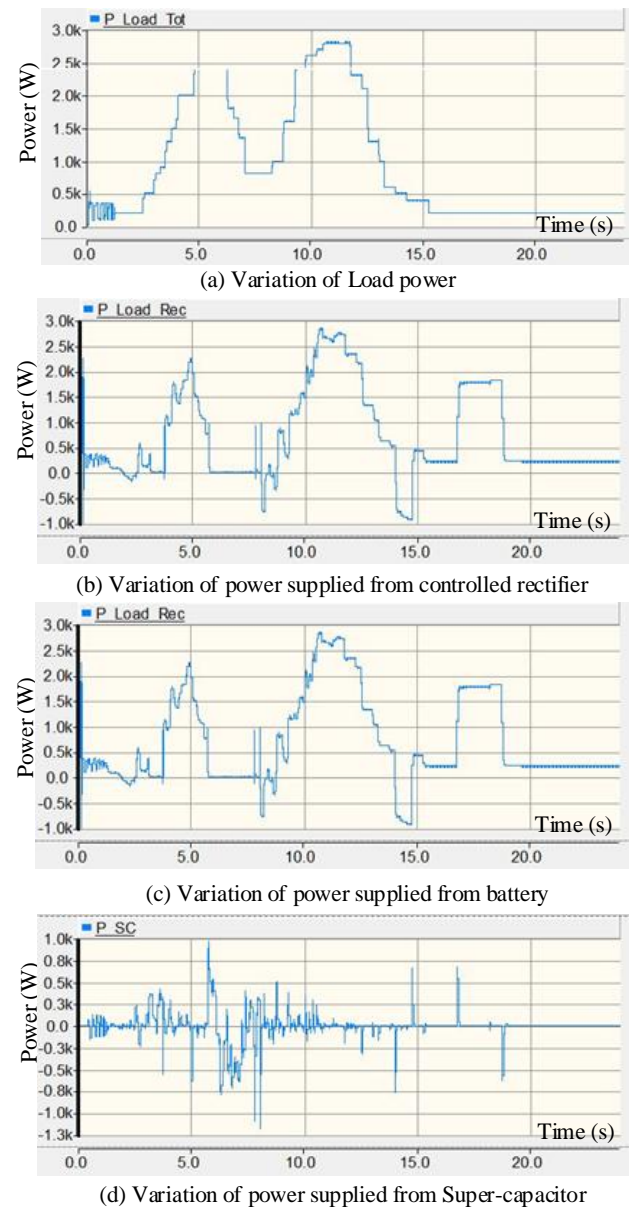

(d) Variation of power supplied from Super-capacitor

Figure 12. Variation of the utility tariff and output power in case study 2

dispatched in 0.5 sec (at 15 min) intervals and in this case the grid failures occurred at the middle of EMS dispatching intervals. Until such time the EMS sends the command to the battery converter, the stability of the dc link was maintained by the super-capacitor converter. This inertia action can be clearly seen in Fig. 12 (d).

VI. CONCLUSIONS

From case studies it was observed that the proposed EMS was capable of handling the power sharing of different energy sources in relation to the demand, under grid connected and islanded modes.

As can be seen from Case study 1, when there is excess power, the EMS scheduled the battery converter either to

150

utilize its energy storage within the MicroGrid or export it to the utility. On the other hand when there is power shortage the EMS scheduled to import power from the ac utility to keep the power balance in more cost effective manner.

Case study 2 demonstrated the operation of the dc MicroGrid under all operating modes of the EMS. The key feature to note here is that the transition of the controls between grid connection and islanding operations. Power sharing between each converter and loads was done seamlessly and MicroGrid controllers handle the power set points according to the schedule dispatched by the EMS. The DSM was effectively utilized to maintain the health of the battery based on a pre-defined SOC level.

The operation of the super-capacitor interface converter helped to minimize the dc link ripples. Also during islanding, it provided the inertia support to the MicroGrid to avoid the collapse.

More importantly the constantly monitoring the degradation of the battery through the discharge cost function is a unique contribution of this piece of work. As the EMS continuously monitors the cost associated with discharging the battery with the utility price, this ensures an optimum utilization of the battery energy storage.

VII. APPENDIX A

Battery Specification [16] from the data sheet of the smart battery, "SB 100"

Parameter	Data
Technology Class	LiFePO4
Nominal Voltage	36.0 V
Rated Capacity	3.3 kWh
Rated DOD	80 %
SOC Max	90%
SOC Min	10%
Number of Cycles	1500
Replacement Cost	Rs.200,000/=

ACKNOWLEDGMENT

REFERENCES

[1] J.-D. Park and J. Candelaria, "Fault Detection and Isolation in Low-Voltage dc-Bus Microgrid System," IEEE Trans. Power Deliv., vol. 28, no. 2, pp. 779–787, 2013

[2] J. M. Guerrero, J. C. Vasquez, J. Matas, L. G. de Vicuña, and M. Castilla, "Hierarchical Control of Droop-Controlled ac and dc Microgrids #x2014;A General Approach Toward Standardization," IEEE Trans. Ind. Electron., vol. 58, no. 1, pp. 158–172, Jan.

[3] C.-M. Lai, C.-T. Pan, and M.-C. Cheng, "High-Efficiency Modular High Step-Up Interleaved Boost Converter for dc-Microgrid Applications," IEEE Trans. Ind. Appl., vol. 48, no. 1, pp. 161–171, 2012.

[4] D. Chen and L. Xu, "Autonomous dc Voltage Control of a dc Microgrid With Multiple Slack Terminals," IEEE Trans. Power Syst., vol. 27, no. 4, pp. 1897–1905, 2012.

[5] Y. Ito, Y. Ito, Y. Zhongqing, and H. Akagi, "dc microgrid based distribution power generation system dc microgrid based distribution power generation system," in Power Electronics and Motion Control Conference, 2004. IPEMC 2004. The 4th International, 2004, vol. 3, pp. 1740–1745 Vol.3.

[6] Y.-K. Chen, Y.-C. Wu, C.-C. Song, and Y.-S. Chen, "Design and Implementation of Energy Management System With Fuzzy Control for dc Microgrid Systems," IEEE Trans. Power Electron., vol. 28, no. 4, pp. 1563–1570, 2013.

[7] H. Kakigano, Y. Miura, and T. Ise, "Distribution Voltage Control for dc Microgrids Using Fuzzy Control and Gain-Scheduling Technique," IEEE Trans. Power Electron., vol. 28, no. 5, pp. 2246–2258, 2013.

[8] J.A.P. Lopes, C.L. Moreira, and A.G. Madureira, "Defining control strategies for MicroGrids islanded operation," IEEE Transactions on Power Systems,, vol. 21, 2006, pp. 916-924.

[9] C.L. Moreira, F.O. Resende, and J.A.P. Lopes, "Using Low Voltage MicroGrids for Service Restoration," IEEE Transactions on Power Systems, vol. 22, 2007, pp. 395-403.

[10] B. Kroposki, R. Lasseter, T. Ise, S. Morozumi, S. Papatlianassiou, and N. Hatziargyriou, "Making microgrids work," IEEE Power and Energy Magazine, vol. 6, 2008, pp. 40-53.

[11] Y. Kojima, M. Koshio, S. Nakamura, H.A.M.H. Maejima, Y.A.F.Y. Fujioka, and T.A.G.T. Goda, "A Demonstration Project in Hachinohe: Microgrid with Private Distribution Line," IEEE International Conference on System of Systems Engineering, SoSE, 2007, pp. 1-6.

[12] A. Yokoyama, "Overview of Microgrid R&D in Japan," Symposium on MicroGrids, University of California, San Diego: 2009.

[13] T. Tsukada, T. Tokumoto, T. Ogata, and S. Tagami, "DEMONSTRATION OF MICROGRID THROUGH THE ACTIVITIES TOWARD HOLONIC ENERGY SYSTEMS," 6th International Conference on Indoor Air Quality, Ventilation & Energy Conservation in Buildings - IAQVEC, Sendai, Japan, 2007: http://www.inive.org/members_area/medias/pdf/Inive%5CIA QVEC2007%5CTsukada.pdf accessed on 2010.02.11, .

[14] A. Denda, "Shimizu's Microgrid Research Activities," Symposium on Microgrids, Canada, 2006: http://der.lbl.gov/new_site/2006microgrids_files/Japan/Presen tation_6_Atsushi_denda.pdf access on 2010.02.11, .

[15] N. Korada and M. K. Mishra, "Grid Adaptive Power Management Strategy for an Integrated Microgrid With Hybrid Energy Storage," IEEE Trans. Ind. Electron., vol. 64, no. 4, pp. 2884–2892, Apr. 2017.

[16] K. Shimomachi, R. Hara, H. Kita, M. Noritake, H. Hoshi, and K. Hirose, "Development of energy management system for DC microgrid for office building:-Day Ahead operation scheduling considering weather scenarios-," in 2014 Power Systems Computation Conference, 2014, pp. 1–6.

[17] I. Tank and S. Mali, "Renewable based DC microgrid with energy management system," in 2015 IEEE International Conference on Signal Processing, Informatics, Communication and Energy Systems (SPICES), 2015, pp. 1–5.

[18] B. Wang, M. Sechilariu, and F. Locment, "Intelligent DC microgrid with smart grid communications: Control strategy consideration and design," in 2013 IEEE Power & Energy Society General Meeting, 2013, pp. 1–1.

[19] R.K. Chauhan, B.S. Rajpurohit, F.M. Gonzalez-Longstt and S.N. Singh, "Intelligent Energy Management System for PV-battery-based Microgrids in future dc homes", International Journal of Emerging Electric Power Systems, Vol 17(3), 2016, pp 339-350.

[20] Yu-Kai Chen, Yung-Chun Wu, Chau-Chung Song, Yu-Syun Chen, "Design and implementation of Energy Management System with fuzy conrol for dc Microgrid system", IEEE Transactions on Power Electronics, Vol 28(4), 2013, pp 1563-1570.

[21] Eun-Kyu Lee, W. Shi, R. Gadh and W. Kim, "Design and implementation of a Microgird Energy Management System", Sustainability. Vol 8, 2016, pp 1-19.

[22] O. Tremblay, "Experimental Validation of a Battery Dynamic Model for EV Applications," World Electr. Veh. J., vol. 3, 2009.

[23] O. Tremblay, L.-A. Dessaint, and A.-I. Dekkiche, "A generic battery model for the dynamic simulation of hybrid electric vehicles," in Proceedings IEEE Vehicle Power and Propulsion Conference, VPPC 2007. Sep. 2007, pp. 284–289.

[24] T. A. Nguyen and M. L. Crow, "Stochastic Optimization of Renewable-Based Microgrid Operation Incorporating Battery Operating Cost," *IEEE Trans. Power Syst.*, vol. 31, no. 3, pp. 2289–2296, May 2016.

[25] Tony Markel and Andrew Simpson, "Plug-in Hybrid Electric Vehicle Energy Storage System Design," presented at the Advanced Automotive Battery Conference, Baltimore, Maryland, 19-May-2006.